

# Blue thermally activated delayed fluorescence emitter using modulated triazines as electron acceptors

Youngnam Lee<sup>a</sup>, Seung-Je Woo<sup>b</sup>, Jang-Joo Kim<sup>b</sup>, Jong-In Hong<sup>a,\*</sup>

<sup>a</sup> Department of Chemistry, Seoul National University, Seoul, 08826, Republic of Korea

<sup>b</sup> Department of Materials Science and Engineering, Seoul National University, Seoul, 08826, Republic of Korea



## ARTICLE INFO

### Keywords:

Organic light emitting diode (OLED)  
Thermally activated delayed fluorescence (TADF)  
Blue emission  
Light out-coupling efficiency  
Emitting dipole orientation

## ABSTRACT

Three types of thermally activated delayed fluorescence (TADF) emitters, namely, **moTrSAC**, **tmTrSAC**, and **motmTrSAC**, are reported that emit blue-shifted emission with high external quantum efficiencies (EQEs). These emitters have electron donating spiroacridine in common and various triazine-based electron acceptors. The electronic and structural control on the electron acceptor moiety adjusts the reduction potential of the molecule to shift the emission wavelength to the blue region. Moreover, as these emitters become widened, the light out-coupling efficiency increases due to the enhanced horizontal emitting dipole orientation. As a result, OLEDs based on **moTrSAC**, **tmTrSAC**, and **motmTrSAC** emit blue light in a range of 460–480 nm with high EQEs of 21.3, 15.5, and 19.5%, respectively.

## 1. Introduction

Thermally activated delayed fluorescence (TADF) has drawn considerable attention, particularly in the field of organic light emitting diodes (OLEDs) because it can enhance the internal quantum efficiency (IQE) to 100% using pure organic materials only [1]. TADF enables overcoming the limitations of fluorescent and phosphorescent molecules developed for the emitting layer (EML) of OLEDs [2–4]. In general, TADF materials consist of distorted electron donor and acceptor groups to reduce the overlap of the highest occupied molecular orbital (HOMO) and lowest unoccupied molecular orbital (LUMO) [5]. Therefore, conversion of the triplet to the singlet state through the reverse intersystem crossing (RISC) is plausible due to the reduced energy gap between the singlet and triplet states ( $\Delta E_{ST}$ ). Red, green, and blue TADF emitters have been developed by introducing various electron donors and acceptors. However, the intrinsic issues of blue emission have retarded the development of blue TADF emitters as compared to red and green emitters [6–10].

The interactions between light and substrates allow for only a restricted number of photons to come out because the light should pass the glass substrate after being emitted from the EML [11,12]. Therefore, the light out-coupling efficiency, which is generally 0.2 in the case of isotropic emitters, should be considered [13,14]. To produce OLEDs with high external quantum efficiencies (EQEs), it is important to not only increase the intrinsic photoluminescence quantum yield (PLQY) of

the emitter itself but also fully extract the light generated in the EML. The light emission from the emitter is mostly perpendicular to its transition dipole moment [15]. When the emitter has a vertical emitting dipole orientation (EDO) to the substrate plane, a large percentage of the light will be trapped in the glass. Thus, to increase the light out-coupling efficiency, emitters should be horizontally oriented. It has been known that the emitter having an anisotropic molecular shape (e.g. linear or planar shape) is arranged horizontally to the substrate to reduce the surface energy of the substrate [16]. Therefore, high efficiency OLEDs can be achieved with anisotropic molecular shapes.

Triazine is a strong electron acceptor having a planar six-membered benzene-like ring but with three carbons replaced by nitrogens. Therefore, triazine has been linked to various electron donors to develop blue-green emitters [17–24]. Recently, spiroacridine has been introduced to TADF emitters as an electron donor due to restricted molecular motions and moderate electron-donating ability [24–28]. The TADF emitter **TrSAC** consists of spiroacridine as an electron donor and 2,4,6-triphenyl-1,3,5-triazine as an electron acceptor [25]. The distorted structure of **TrSAC** between spiroacridine and a phenylene spacer separates the HOMO and LUMO, resulting in efficient TADF emission as well as enhanced PLQY. **TrSAC** also exhibits high EQE due to efficient light extraction resulting from the horizontal orientation of its linear shape. We expect that the structural modification of the triazine acceptor unit of sky-blue emitting **TrSAC** would push the emission wavelength to the blue region.

\* Corresponding author.

E-mail addresses: [jjkim@snu.ac.kr](mailto:jjkim@snu.ac.kr) (J.-J. Kim), [jihong@snu.ac.kr](mailto:jihong@snu.ac.kr) (J.-I. Hong).

<https://doi.org/10.1016/j.dyepig.2019.107864>

Received 2 August 2019; Received in revised form 5 September 2019; Accepted 5 September 2019

Available online 05 September 2019

0143-7208/ © 2019 Elsevier Ltd. All rights reserved.

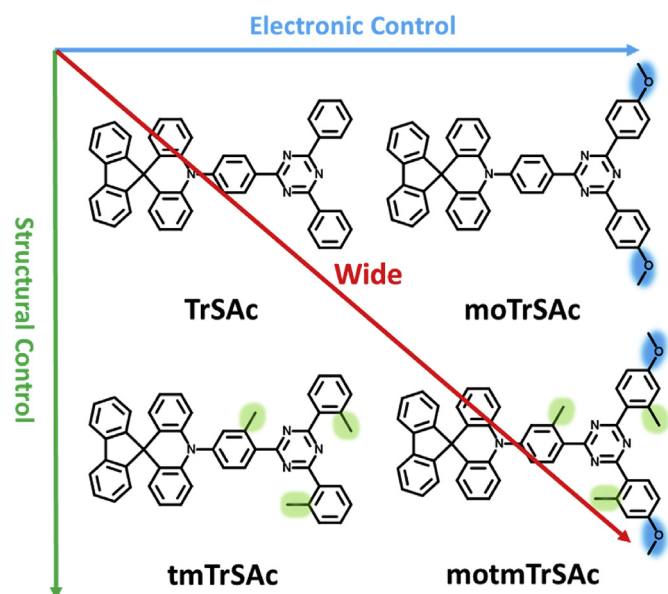


Fig. 1. Design concept of the TADF emitters with modulated triazines.

Herein, we report three blue TADF emitters, **moTrSAC**, **tmTrSAC** and **motmTrSAC**, which were designed through the electronic and structural modulation of the triphenyltriazine unit (Fig. 1). These modulations did not affect the TADF, but led to a blue-shifted emission and enhanced horizontal EDO as compared to **TrSAC**. Results show that the OLED devices based on the modulated triazines shifted the CIE color coordinates to the blue region with fairly good EQEs by enhanced light out-coupling efficiency. **moTrSAC**, **tmTrSAC**, and **motmTrSAC**-based devices showed CIE color coordinates of (0.17, 0.27), (0.17, 0.27), and (0.16, 0.22) and EQEs of 21.3, 15.5, and 19.5%, respectively. These results suggest that electronic and structural modulation of triazine-based electron acceptors can be a strategy to shift the emission wavelength and increase light out-coupling efficiency.

## 2. Results and discussion

### 2.1. Theoretical calculations

We calculated the optimized molecular structures and energies of the frontier molecular orbitals through density functional theory (DFT) calculations at the B3LYP/6-31G(d) level using Gaussian 09. Calculated data are presented in Fig. 2 and summarized in Table 1. The optimized molecular structures showed the distorted shape due to the steric hindrance between spiroacridine and the phenylene spacer. The HOMO

and LUMO were distributed on the spiroacridine and triaryltriazine units, respectively. Because of the poor HOMO LUMO overlap, **moTrSAC**, **tmTrSAC**, and **motmTrSAC** exhibited a small  $\Delta E_{ST}$  value of 0.01 eV, which is identical to that of **TrSAC**. The result indicates that modulations on the triphenyltriazine unit have little effect on the TADF. TADF emitter **moTrSAC** with *p*-methoxy substitution on the terminal diphenyltriazine moiety showed higher LUMO (1.80 eV) than that of **TrSAC** (2.01 eV) because of the electron-donating ability of the methoxy group. The triazine of **tmTrSAC** was distorted by  $27^\circ$  with respect to the central methylphenylene linker due to the methyl substitution, which caused destabilization of the conjugation. Consequently, **tmTrSAC** with deconjugated tri(*o*-tolyl)triazine elevated the LUMO (1.87 eV) as compared to the methyl-free **TrSAC** (2.01 eV). In other words, methoxy and methyl substitutions raised the LUMO energy by 0.21 and 0.14 eV in **moTrSAC** and **tmTrSAC**, respectively. The methyl substitution in the linker and acceptor elevated the LUMO by 0.06 and 0.08 eV, respectively (see Fig. S1 and Table S1). In the case of **motmTrSAC**, the simultaneous introduction of methoxy and methyl groups raised the LUMO (0.21 eV + 0.14 eV), resulting in the highest LUMO (1.66 eV) and  $E_{gap}$  among the triazine series. Therefore, the electronic and structural modulation allowed the emission wavelength to be shifted into the blue region through an increase in the  $E_{gap}$ .

### 2.2. Synthesis

The synthetic strategy employed to obtain the three emitters is illustrated in Scheme 1, where **1**, **2**, and **3** were synthesized according to the previous report [29]. The bromine-lithium exchange reaction of **2** and **3** with *n*-butyllithium (*n*-BuLi) followed by transmetalation with trimethyl borate furnished **4** and **5**, respectively. The reaction of cyanuric chloride with Grignard reagents prepared from monoaryl bromides afforded the diaryltriazine compounds (**6**, **7**, and **8**). The Suzuki-Miyaura cross-coupling reaction between appropriate boronic acid (**4**, **5**) and diaryltriazine compounds (**6**, **7**, **8**) provided **moTrSAC**, **tmTrSAC**, and **motmTrSAC**. The three emitters were purified by column chromatography, followed by recrystallization and temperature-gradient sublimation. Their chemical structures were fully characterized by  $^1\text{H}$  NMR,  $^{13}\text{C}$  NMR, elemental analysis, and high-resolution mass spectrometry.

### 2.3. Electrochemical properties

The electrochemical properties of these compounds were analyzed using cyclic voltammetry (CV), and their corresponding voltammograms are presented in Fig. 3a and b and summarized in Table 2. The oxidation potentials of **moTrSAC**, **tmTrSAC**, and **motmTrSAC** were nearly identical to that of **TrSAC** because they have the same electron donors. The HOMO energy levels were calculated from the onset of the

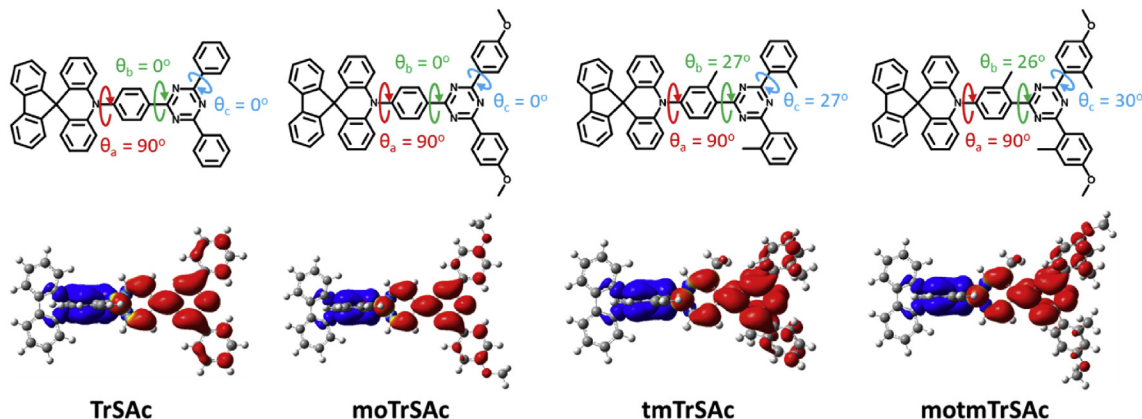


Fig. 2. Optimized molecular structures.

**Table 1**  
Calculated data.

	HOMO[eV]	LUMO [eV]	E <sub>gap</sub> [eV]	E <sub>Singlet</sub> [eV]	E <sub>Triplet</sub> [eV]	ΔE <sub>ST</sub> [eV]	θ <sub>a</sub> [°]	θ <sub>b</sub> [°]	θ <sub>c</sub> [°]
TrSAc	4.96 eV	2.01 eV	2.95 eV	2.43 eV	2.42 eV	0.01 eV	90	0	0
moTrSAc	4.90 eV	1.80 eV	3.10 eV	2.57 eV	2.56 eV	0.01 eV	90	0	0
tmTrSAc	4.93 eV	1.87 eV	3.06 eV	2.55 eV	2.54 eV	0.01 eV	90	27	27
motmTrSAc	4.87 eV	1.66 eV	3.21 eV	2.68 eV	2.67 eV	0.01 eV	90	26	30

spectra and found to be 5.35 eV for all these molecules. However, the reduction potentials were different depending on the electronic and structural modulations. The LUMO energy levels of **moTrSAc** and **tmTrSAc** (2.75 eV) were 0.1 eV higher than that of **TrSAc** (2.85 eV). Therefore, substitution of two methoxy groups and three methyl groups in **motmTrSAc** further elevated its LUMO energy level (2.65 eV) by the summation of electrical and structural variations. Therefore, we expected that the adjustment of the LUMO energy by electrical and structural modulations could shift the emission wavelength to the blue region.

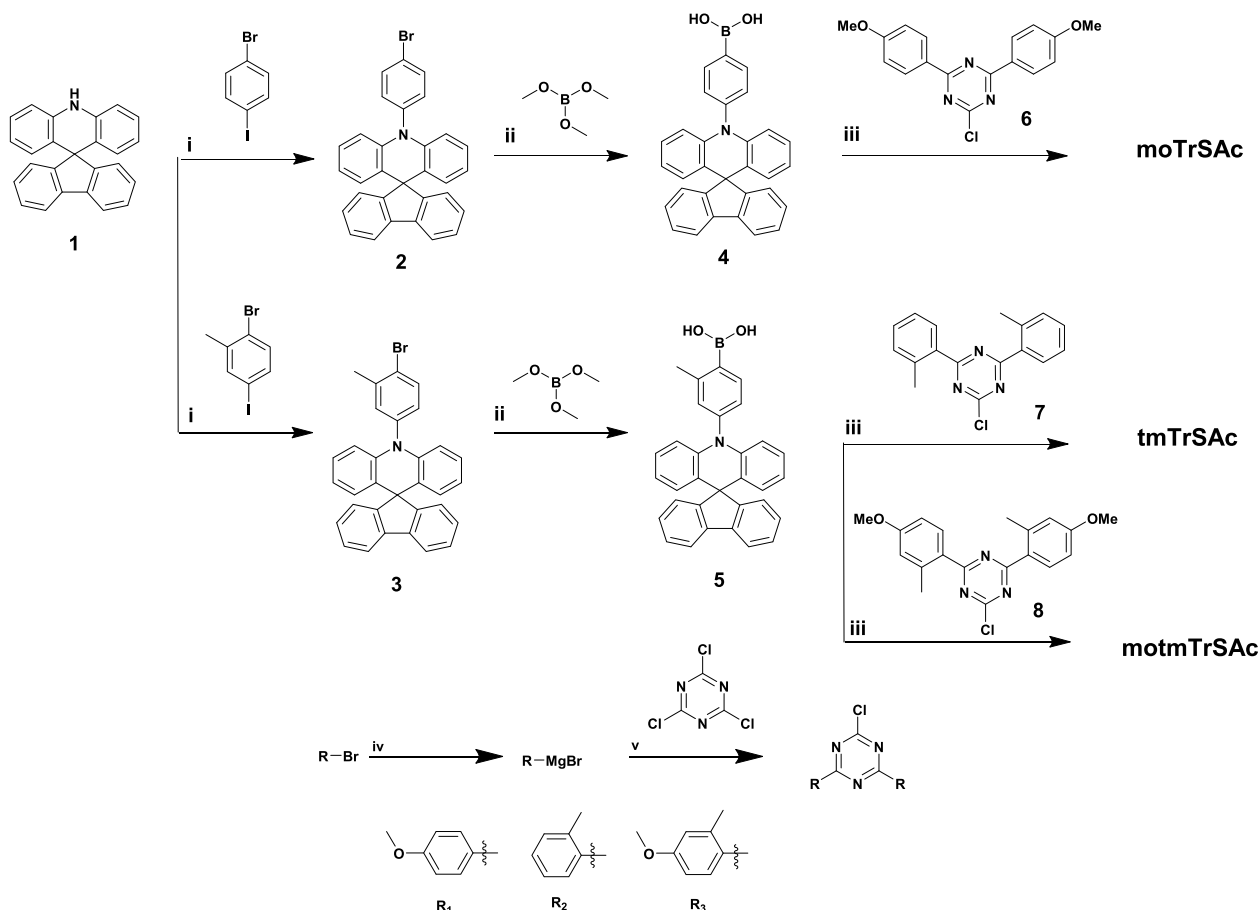
#### 2.4. Photophysical properties

Photophysical properties of **TrSAc**, **moTrSAc**, **tmTrSAc**, and **motmTrSAc** were evaluated using ultraviolet–visible (UV–Vis) absorption, photoluminescence (PL), time-resolved PL, and angle-dependent PL measurements. As shown in the UV–Vis spectra, the absorption peaks at 350–450 nm indicate the intramolecular charge transfer (CT) transition between the electron donor and acceptor in each emitter (**Fig. 3c**). The emission spectral shift depending on the solvent polarity

further proves CT character (**Fig. S2**). The PL spectra of **moTrSAc**, **tmTrSAc**, and **motmTrSAc** in toluene solution showed emission wavelengths of 476, 470, and 467 nm, respectively (**Fig. 3c**). As predicted from the DFT calculations and CV data, the emission wavelengths moved to the blue region as compared to **TrSAc** (λ = 484 nm) because of the widened E<sub>gap</sub>.

PL measurements performed at 300 and 77 K in toluene revealed the singlet and triplet characteristics, respectively (**Fig. S3**). The singlet and triplet energies were calculated from the onset of the spectra and are summarized in **Table 2**. The fluorescence and phosphorescence spectra of **TrSAc**, **moTrSAc**, **tmTrSAc**, and **motmTrSAc** overlapped significantly, indicating a small ΔE<sub>ST</sub>. Therefore, TADF emission was expected in **moTrSAc**, **tmTrSAc**, and **motmTrSAc** as was observed in **TrSAc** because the ΔE<sub>ST</sub> values of **moTrSAc**, **tmTrSAc**, and **motmTrSAc** were also significantly low (~0.01 eV).

Photophysical properties of thin films were also investigated. All films were fabricated by doping 10 wt% emitter using bis[2-(diphenylphosphino)phenyl] ether oxide (DPEPO) as a host with high triplet energy [30]. The emission wavelength of films was shifted to a blue region in a similar manner as was observed in solution (**Fig. 3d**).



**Scheme 1.** Synthetic routes for **moTrSAc**, **tmTrSAc**, and **motmTrSAc**. (i) CuI, 1,2-diaminocyclohexane, K<sub>2</sub>CO<sub>3</sub>, 1,4-dioxane, 100 °C; (ii) *n*-BuLi, THF, -78 °C; (iii) Pd(PPh<sub>3</sub>)<sub>4</sub>, K<sub>2</sub>CO<sub>3</sub>, toluene/H<sub>2</sub>O, 100 °C; (iv) I<sub>2</sub>, Mg, THF, 70 °C, 3 h; (v) THF, 50 °C, 12 h (R<sub>1</sub> = **6**, R<sub>2</sub> = **7**, R<sub>3</sub> = **8**).

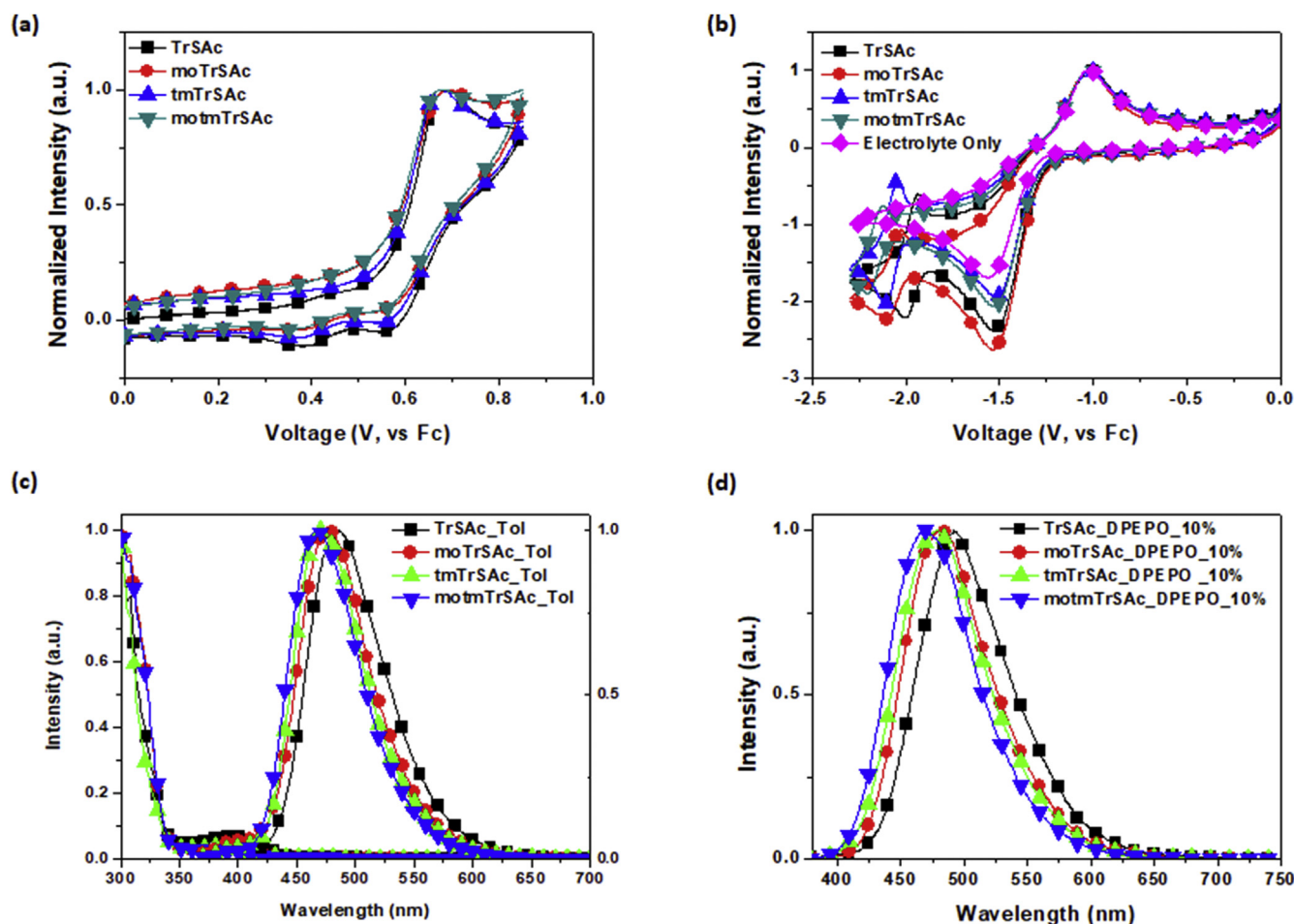


Fig. 3. (a) Oxidation potential curves, (b) reduction potential curves, (c) absorption and emission spectra in toluene ( $10^{-5}$  M), (d) emission spectra of 10 wt% doped film in DPEPO of TrSAc, tmTrSAc, moTrSAc, and motmTrSAc.

However, because of the polarity of DPEPO, the emission wavelengths of films were red-shifted compared to those of the toluene solution state [17,26]. moTrSAc, tmTrSAc, and motmTrSAc showed lower PLQYs of 70, 62, and 51% in the film state, respectively, as compared to TrSAc (80.1%) [27], presumably because of decreased CT character and adjusted vibrational modes [22,31,32].

Fig. 4 shows the transient PL curves in film states, and lifetimes are summarized in Table 2. Transient PL measurements of the thin films of four emitters exhibited bi-exponential decays with the prompt and delayed fluorescence components, which indicates that all emitters efficiently underwent ISC to the triplet state and RISC from the triplet state. These results confirmed that electronic and structural modulations of the triaryltriazine moiety maintained the TADF characteristics.

Angle-dependent PL of 10 wt% doped films in DPEPO was measured to determine the EDO of TrSAc, moTrSAc, tmTrSAc, and motmTrSAc

(Fig. 5). Linear-shaped TrSAc itself showed the horizontal EDO of 78%, which is different from the horizontal EDO values in mCPN and mCP/TSP01 hosts due to different host-guest interactions [24,25,33]. Methoxy-substituted moTrSAc and methyl-substituted tmTrSAc showed enhanced horizontal EDOs of 85% and 80%, respectively, because of widened molecular shapes compared to TrSAc [16]. Of the three emitters, motmTrSAc having both methoxy and methyl groups exhibited the highest horizontal EDO of 88%. As a result, despite relatively low PLQYs of moTrSAc, tmTrSAc, and motmTrSAc with blue-shifted emission, their OLED devices could maintain high efficiencies because of the enhanced horizontal dipole orientation.

## 2.5. Thermal properties

Thermogravimetric analysis (TGA) of moTrSAc, tmTrSAc, and

Table 2  
Electrochemical and photophysical data.

	HOMO <sup>a</sup> [eV]	LUMO <sup>a</sup> [eV]	$\lambda_{\text{Max}}^{\text{b/c}}$ , [nm]	PLQY <sup>c</sup> [%]	$S_1^{\text{b}}$ [eV]	$T_1^{\text{b}}$ [eV]	$\Delta E_{\text{ST}}^{\text{b}}$ [eV]	$\tau_1^{\text{c}}$ [ns]	$\tau_2^{\text{c}}$ [ $\mu$ s]	$\theta/\text{d}^{\text{d}}$ [%]
TrSAc	5.35	2.85	484/492	80.1	2.87	2.86	0.01	33	1.6	78
moTrSAc	5.35	2.75	470/482	70	2.94	2.93	0.01	29	3.4	85
tmTrSAc	5.35	2.75	476/479	62	2.96	2.95	0.01	24	2.5	80
motmTrSAc	5.35	2.65	467/469	51	2.97	2.96	0.01	31	3.0	88

<sup>a</sup> Estimated from the onset potentials ( $^{\text{ox}}E_{\text{onset}}$  and  $^{\text{red}}E_{\text{onset}}$  [eV] against Fc/Fc<sup>+</sup> redox couple) in CV experiments.

<sup>b</sup> Measured in toluene solution ( $10^{-5}$  M).

<sup>c</sup> Measured using 10 wt% doped films in DPEPO.

<sup>d</sup> Horizontal emitting dipole ratio.

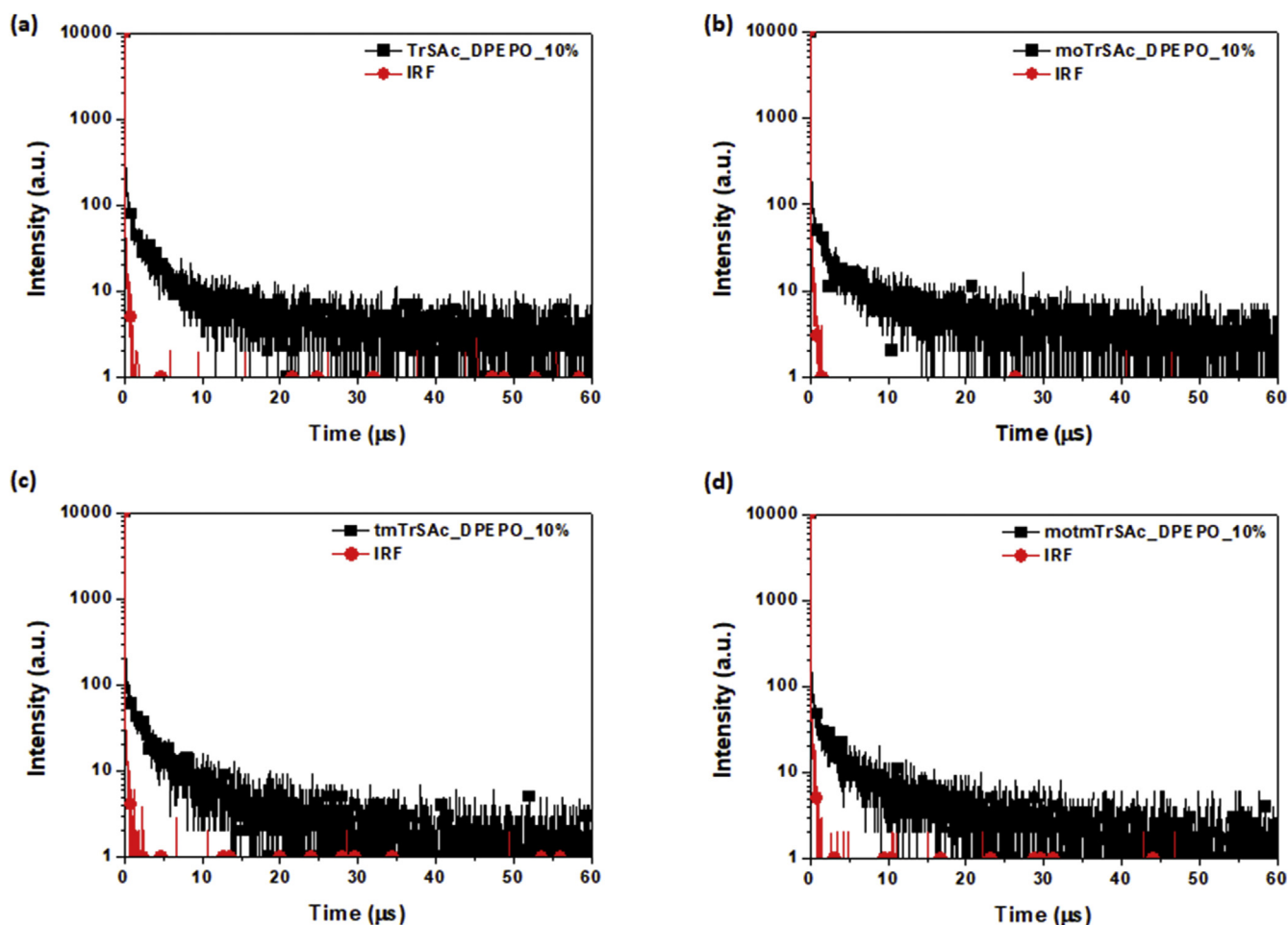


Fig. 4. Transient-PL decay curves of 10 wt% in DPEPO film of (a) TrSAC, (b) moTrSAC, (c) tmTrSAC, and (d) motmTrSAC.

motmTrSAC was conducted to measure the thermal decomposition temperature ( $T_d$ ).  $T_d$  of moTrSAC, tmTrSAC, and motmTrSAC were 423, 384, and 409 °C, respectively. All these emitters showed higher thermal stability than that of TrSAC (381 °C). The TGA thermograms of the emitters are presented in Fig. S4.

## 2.6. Device properties

Multilayer devices were fabricated based on TrSAC, moTrSAC, tmTrSAC, and motmTrSAC to verify the OLED characteristics as follows (Fig. 6a): ITO (150 nm)/N,N'-bis(naphthalen-1-yl)-N,N'-bis(phenyl) benzidine (NPB, 80 nm)/1,3-di(9H-carbazol-9-yl)benzene (mCP, 10 nm)/DPEPO: emitter (10 wt%, 20 nm)/DPEPO (10 nm)/2,2',2''-(1,3,5- benzenetriyl)-tris(1-phenyl-1H-benzimidazole) (TPBi, 40 nm)/LiF (1 nm)/Al (100 nm). The device data are summarized in Table 3. The devices of TrSAC, moTrSAC, tmTrSAC and motmTrSAC showed emission maxima at 484, 476, 472 nm, and 468 nm, respectively (Fig. 6b). Emission wavelengths were shifted to the blue region as expected from the photophysical characteristics when the methoxy and methyl groups were introduced on the triphenyltriazine. Although the color coordinates of TrSAC were in the sky blue to green region, those of moTrSAC, tmTrSAC, and motmTrSAC were in the blue region with y coordinates under 0.3. The device efficiency of TrSAC, moTrSAC, tmTrSAC, and motmTrSAC was 23.8, 21.3, 15.5, and 19.5%, respectively (Fig. 6d). motmTrSAC was expected to have the lowest EQE because of the lowest PLQY with the emission wavelength shifted to the blue region. However, motmTrSAC showed better efficiency than that of tmTrSAC because motmTrSAC had the highest degree of horizontal dipole orientation. This suggests that high EQEs can be obtained even

with decreased PLQY by increasing the light out-coupling efficiency.

## 3. Conclusion

We synthesized triazine-based TADF emitters moTrSAC, tmTrSAC, and motmTrSAC with spiroacridine as the electron donor and modulated triazines as the acceptor. Modulations of the triazine moiety shifted the emission wavelength to the blue region while maintaining the TADF characteristics. Moreover, as the shape of the emitters became more planar, the horizontal dipole orientation increased, resulting in enhanced light out-coupling efficiency. Results show that the OLEDs based on moTrSAC, tmTrSAC, and motmTrSAC had EQEs of 21.3, 15.5, and 19.5%, respectively. These results indicated that modulation of the triazine electron acceptor moiety can be a strategy to shift the emission wavelength to the blue region and enhance the light out-coupling efficiencies.

## 4. Experimental

### 4.1. Quantum chemical calculations

All quantum chemical calculations were performed using Gaussian 09 program package. Geometry optimizations and energy calculations for the lowest excited singlet and triplet states were carried out using DFT and time-dependent DFT calculations at the B3LYP/6-31G(d) level.

### 4.2. Synthesis and characterization

Commercially available reagents and solvents were used without

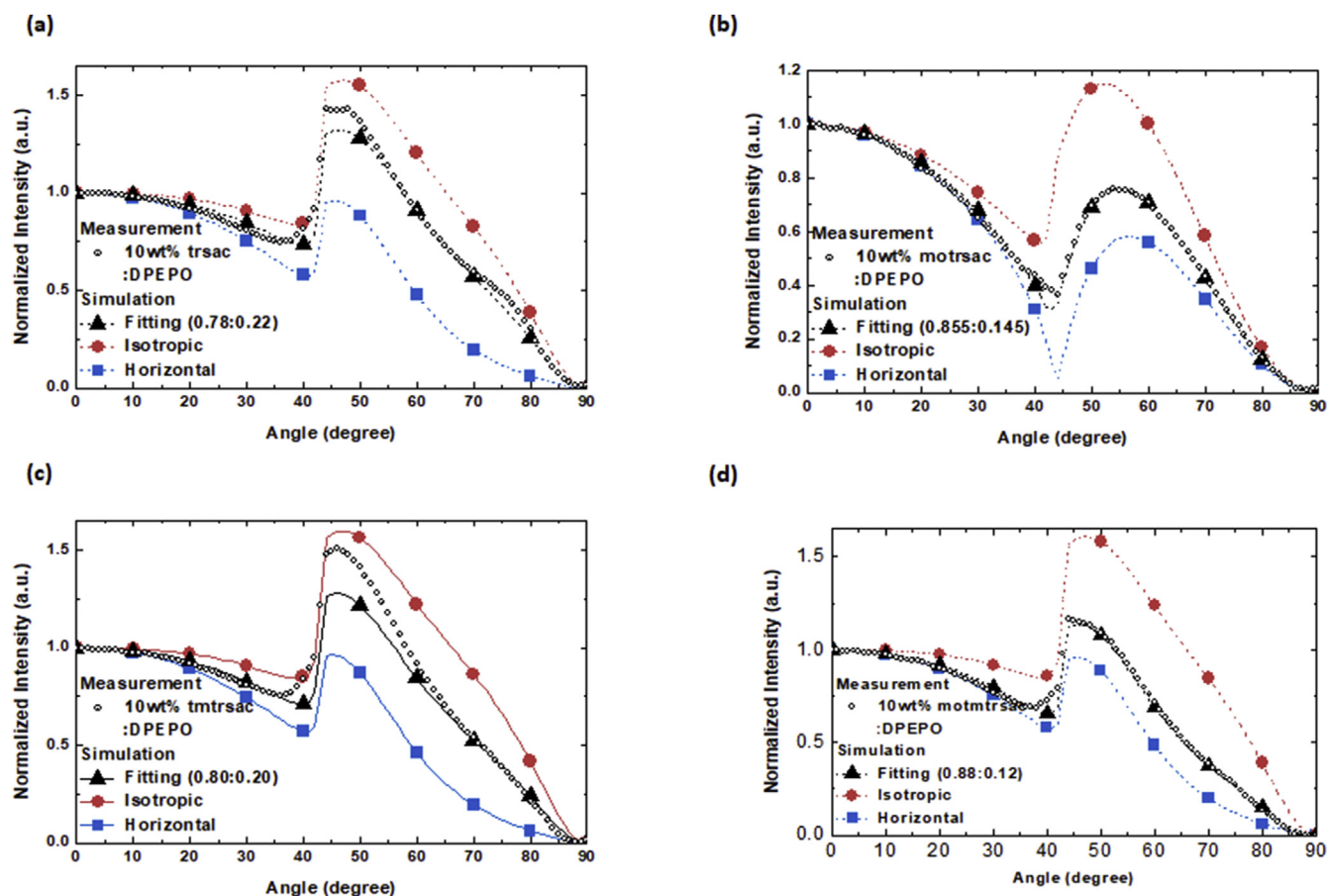


Fig. 5. Angle-dependent PL intensities of (a) TrSAC, (b) moTrSAC, (c) tmTrSAC, and (d) motmTrSAC.

further purification unless otherwise noted.  $^1\text{H}$  and  $^{13}\text{C}$  NMR spectra were recorded using Agilent 400-MR DD2 400 MHz or Varian/Oxford As-500 500 MHz in  $\text{CDCl}_3$ .  $^1\text{H}$  NMR chemical shifts in  $\text{CDCl}_3$  were referenced to  $\text{CHCl}_3$  (7.27 ppm).  $^{13}\text{C}$  NMR chemical shifts in  $\text{CDCl}_3$  were reported relative to  $\text{CHCl}_3$  (77.23 ppm). High-resolution mass spectrometric data (JEOL, JMS-700) with electron impact (EI) and fast atom bombardment (FAB) positive mode were received directly from the National Centre for Inter-University Research Facilities. Elemental analyses were carried out using a Thermo Scientific FlashEA 1112.

#### 4.3. Electrochemical and thermal analysis

Cyclic voltammetry (CV) experiments were conducted using CH instruments 650B electrochemical analyzer in DMF solution (1.00 mM) with 0.1 M tetrabutylammonium perchlorate (TBAP) as the supporting electrolyte. A glassy carbon electrode was employed as the working electrode and referenced to the Ag reference electrode. All potential values were calibrated against the ferrocene/ferrocenium ( $\text{Fc}/\text{Fc}^+$ ) redox couple. The onset potential was determined from the intersection of two tangents drawn at the rising and background current of the cyclic voltammogram. Thermal analyses were performed with TA instrument Q50 thermogravimetric analyzer in nitrogen atmosphere at heating rate of  $10\text{ }^\circ\text{C min}^{-1}$ .

#### 4.4. Photophysical property analysis

UV-visible spectra were recorded with Jasco V-730 spectrometer. Fluorescence and phosphorescence spectra were recorded with Jasco FP-8300 spectrophotometer. PLQYs were measured using monochromator-attached photomultiplier tube (PMT) with a PL sample in an integrating sphere using continuous wave 325 nm He/Cd laser for

excitation. Photoluminescence decay traces were obtained through the time-correlated single photon counting (TCSPC) techniques by using a PicoQuant, FluoTime 250 instrument. 377 nm pulsed laser was used as an excitation source. For angle-dependent PL (ADPL) measurements, polarized lights emitted from PL samples were measured by attaching the film substrate to half-cylinder lens with index-matching oil and changing the angle between the sample and the detector from  $-90^\circ$  to  $90^\circ$  using a motorized rotational stage.

#### 4.5. Device fabrication and measurements

The patterned ITO (150 nm) substrates were washed with water and isopropyl alcohol, followed by 10 min UV-ozone treatment. Organic layers, LiF, and Al were thermally evaporated at a deposition rate of  $1\text{--}2\text{ \AA s}^{-1}$  for organic layers,  $0.1\text{ \AA s}^{-1}$  for LiF, and  $3\text{--}5\text{ \AA s}^{-1}$  for the Al electrode. OLED properties were measured using Keithley source meter 2400 and PR-650 spectrascan colorimeter.

#### 4.6. Materials

##### 4.6.1. Synthesis of 10H-spiro[acridine-9,9'-fluorene] (1, SAc)

1 was prepared according to the literature procedure [20]. Compound 1 (11.60 g, 40%) was obtained as a white powder.

##### 4.6.2. Synthesis of 10-(4-bromophenyl)-10H-spiro[acridine-9,9'-fluorene] (2)

2 was prepared according to the literature procedure [20]. Compound 2 (2.4 g, 54.5%) was obtained as a white solid.

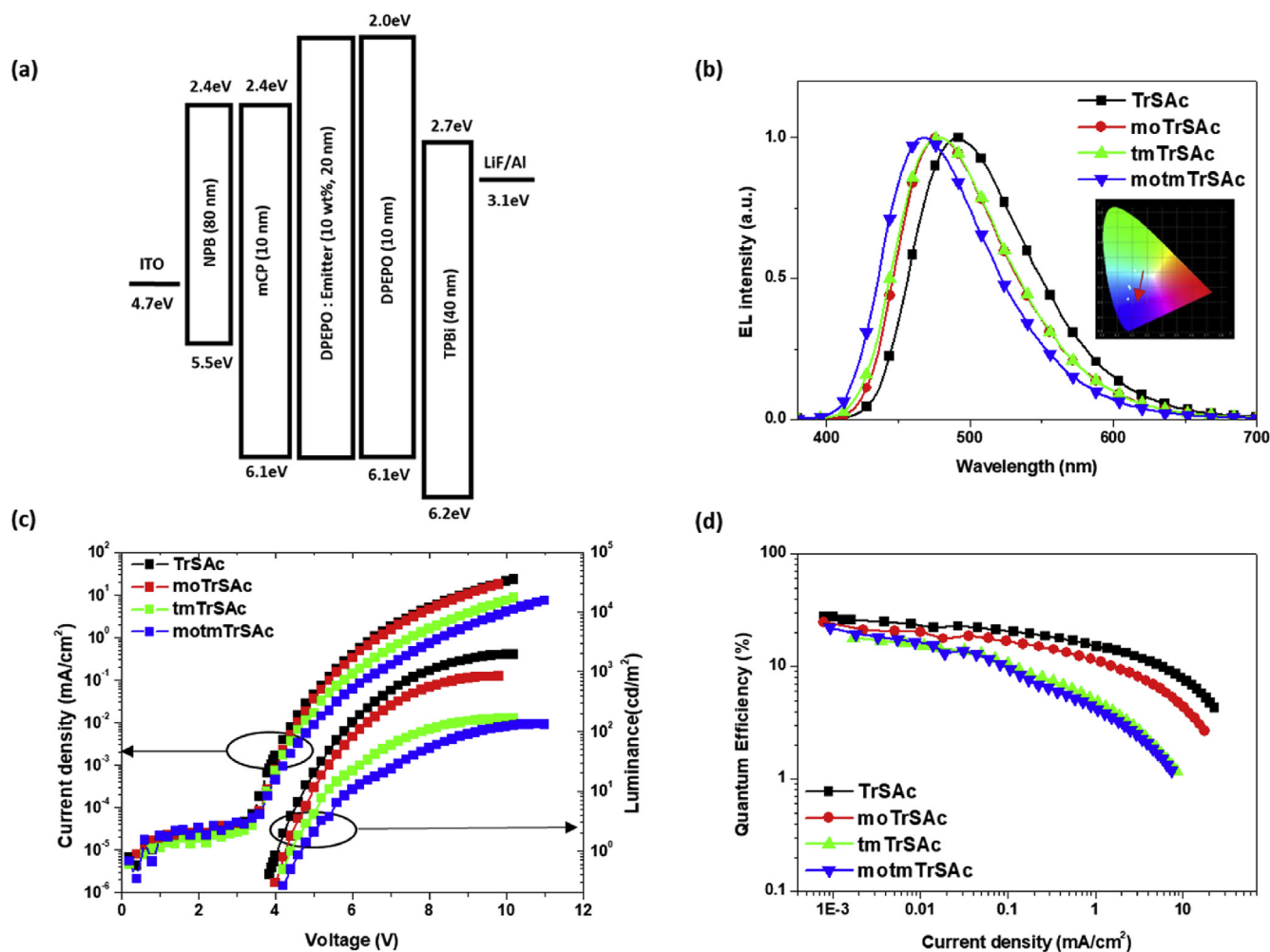


Fig. 6. (a) Device structure, (b) EL spectra (inset: color coordinates), (c) current density-voltage-luminance (J-V-L) spectra, (d) external quantum efficiency-current density ( $\eta_{EQE}$ -J) spectra. (For interpretation of the references to color in this figure legend, the reader is referred to the Web version of this article.)

Table 3  
Summarized device data.

	Turn on Voltage (V)	EQE <sub>Max</sub> <sup>a</sup> (%)	CE <sup>b</sup> (cd A <sup>-1</sup> )	PE <sup>c</sup> (lm W <sup>-1</sup> )	CIE <sup>d</sup> Coordinates (x, y)	$\lambda_{max}$ <sup>e</sup> (nm)
TrSAc	3.9	23.8	50.1	40.9	0.19,0.36	484
moTrSAc	4.2	21.3	36.6	28.7	0.17,0.27	472
tmTrSAc	4.0	15.5	28.5	21.3	0.17,0.27	476
motmTrSAc	4.2	19.5	29.2	21.8	0.16,0.22	468

<sup>a</sup> External quantum efficiency.

<sup>b</sup> Current efficiency.

<sup>c</sup> Power efficiency.

<sup>d</sup> CIE 1931 color coordinates.

<sup>e</sup> Emission wavelength at 5 V.

#### 4.6.3. Synthesis of 10-(4-bromo-3-methylphenyl)-10H-spiro[acridine-9,9'-fluorene] (3)

A mixture of 10H-spiro[acridine-9,9'-fluorene] (1) (4.50 g, 13.60 mmol), 1-bromo-4-iodo-2-methylbenzene (4.45 g, 15 mmol), copper iodide (260 mg, 0.136 mmol), ( $\pm$ )-*trans*-1,2-diaminocyclohexane (0.34 mL, 2.8 mmol) and sodium *tert*-butoxide (2.60 g, 2.80 mmol) in 1,4-dioxane (15 mL) was refluxed overnight under a nitrogen atmosphere. The reaction mixture was then filtered through a pad of silica and extracted with chloroform. The organic layer was washed with water and brine, and dried over anhydrous sodium sulfate. The filtrate was concentrated *in vacuo* to give a crude mixture, which

was purified by column chromatography (SiO<sub>2</sub>, CHCl<sub>3</sub>:hexane = 1:4) to afford compound **3** (2.4 g, 54.5%) as a white solid.

<sup>1</sup>H NMR (400 MHz, CDCl<sub>3</sub>)  $\delta$  (ppm): 7.87 (d,  $J$  = 8.3 Hz, 1H), 7.80 (d,  $J$  = 7.6 Hz, 2H), 7.43–7.32 (m, 5H), 7.28–7.18 (m, 3H), 6.97–6.89 (m, 2H), 6.60–6.52 (m, 2H), 6.46–6.30 (m, 4H), 2.54 (s, 3H). <sup>13</sup>C NMR (100 MHz, CDCl<sub>3</sub>)  $\delta$  (ppm): 156.55, 141.22, 140.97, 140.20, 139.18, 134.94, 133.41, 130.11, 128.35, 127.86, 127.58, 127.20, 125.73, 124.77, 120.71, 119.89, 114.50, 56.72, 23.16.

#### 4.6.4. Synthesis of (4-(10H-spiro[acridine-9,9'-fluorene]-10-yl)phenyl)boronic acid (4)

10-(4-bromophenyl)-10H-spiro[acridine-9,9'-fluorene] (1.08 g, 2.05 mmol) (**2**) was dissolved in dry THF (82 mL) under a nitrogen atmosphere. This solution was cooled to  $-78$  °C followed by dropwise addition of 1.6 M *n*-butyl lithium solution in hexane (1.9 mL, 3.08 mmol). This mixture was stirred for 2 h after which trimethylborate (0.46 mL, 4.1 mmol) was added. After stirring at room temperature overnight, the reaction mixture was added to an aqueous HCl solution (1 N) and extracted with chloroform. The combined organic extracts were dried over sodium sulfate, concentrated *in vacuo* to afford compound **4**. **4** was used for the next reaction without further purification.

#### 4.6.5. Synthesis of (2-methyl-4-(10H-spiro[acridine-9,9'-fluorene]-10-yl)phenyl)boronic acid (5)

10-(4-bromo-3-methylphenyl)-10H-spiro[acridine-9,9'-fluorene] (4.2 g, 8.40 mmol) (**3**) was dissolved in dry THF (168 mL) under a

nitrogen atmosphere. This solution was cooled to  $-78^{\circ}\text{C}$  followed by dropwise addition of 1.6 M *n*-butyl lithium solution in hexane (7.9 mL, 12.6 mmol). The mixture was stirred for 2 h after which trimethylborate (1.9 mL, 16.8 mmol) was added. After stirring at room temperature overnight, the reaction mixture was added to an aqueous HCl solution (1 N) and extracted with chloroform. The combined organic extracts were dried over sodium sulfate, concentrated *in vacuo* to afford compound **5**, which was used in the next reaction without further purification.

#### 4.6.6. Synthesis of 10-(4-(4,6-bis(4-methoxyphenyl)-1,3,5-triazin-2-yl)phenyl)-10H-spiro[acridine-9,9'-fluorene] (moTrSAc)

A mixture of 2-chloro-4,6-bis(4-methoxyphenyl)-1,3,5-triazine (**6**) (583 mg, 1.78 mmol), (4-(10H-spiro[acridine-9,9'-fluorene]-10-yl)phenyl)boronic acid (**4**) (960 mg, 2.13 mmol), tetrakis(triphenylphosphine)palladium(0) (104 mg, 0.09 mmol) and potassium carbonate (492 mg, 3.56 mmol) in toluene (18 mL) and water (4 mL) was refluxed overnight under a nitrogen atmosphere. The reaction mixture was then filtered through a pad of silica and extracted with chloroform. The organic layer was washed with water and brine, and dried using anhydrous sodium sulfate. The filtrate was concentrated *in vacuo* to give a crude mixture, which was purified by column chromatography ( $\text{SiO}_2$ ,  $\text{CHCl}_3$ : hexane = 2 : 1) to afford compound **moTrSAc** (970 mg, 78%) as a yellow solid.

$^1\text{H}$  NMR (400 MHz,  $\text{CDCl}_3$ )  $\delta$  (ppm): 9.06 (d,  $J = 8.4$  Hz, 2H), 8.77 (d,  $J = 8.9$  Hz, 4H), 7.80 (d,  $J = 7.5$  Hz, 2H), 7.70 (d,  $J = 8.4$  Hz, 2H), 7.46 (d,  $J = 7.5$  Hz, 2H), 7.38 (t,  $J = 7.4$  Hz, 2H), 7.27 (t,  $J = 8.0$  Hz, 2H), 7.09 (d,  $J = 8.9$  Hz, 4H), 6.99–6.85 (m, 2H), 6.58 (t,  $J = 7.4$  Hz, 2H), 6.50–6.37 (m, 4H), 3.94 (s, 6H).  $^{13}\text{C}$  NMR (101 MHz,  $\text{CDCl}_3$ )  $\delta$  (ppm): 171.16, 170.53, 163.37, 156.50, 144.76, 140.98, 139.20, 136.79, 131.63, 131.47, 130.86, 128.72, 128.37, 127.84, 127.58, 127.25, 125.77, 124.86, 120.74, 119.88, 114.62, 113.99, 56.78, 55.46. Elem. Anal. calcd for  $\text{C}_{48}\text{H}_{34}\text{N}_4\text{O}_2$  C 82.50, H 4.90, N 8.02; found C 82.56, H 4.88, N 8.04, HRMS (FAB+): calcd for  $\text{C}_{48}\text{H}_{34}\text{N}_4\text{O}_2$   $[\text{M}]^+$ : 698.2682; found: 698.2678.

#### 4.6.7. Synthesis of 10-(4-(4,6-di-*o*-tolyl-1,3,5-triazin-2-yl)-3-methylphenyl)-10H-spiro[acridine-9,9'-fluorene] (tmTrSAc)

A mixture of 2-chloro-4,6-di-*o*-tolyl-1,3,5-triazine (**7**) (426 mg, 1.44 mmol), (2-methyl-4-(10H-spiro[acridine-9,9'-fluorene]-10-yl)phenyl)boronic acid (**5**) (805 mg, 1.73 mmol), tetrakis(triphenylphosphine)palladium(0) (81 g, 0.07 mmol) and potassium carbonate (400 mg, 2.88 mmol) in toluene (14 mL) and water (3 mL) was refluxed overnight under a nitrogen atmosphere. The reaction mixture was then filtered through a pad of silica and extracted with chloroform. The organic layer was washed with water and brine, and dried using anhydrous sodium sulfate. The filtrate was concentrated *in vacuo* to give a crude mixture, which was purified by column chromatography ( $\text{SiO}_2$ ,  $\text{CHCl}_3$ : hexane = 1 : 2) to afford compound **tmTrSAc** (860 mg, 88%) as a yellow solid.

$^1\text{H}$  NMR (499 MHz,  $\text{CDCl}_3$ )  $\delta$  (ppm): 8.59 (d,  $J = 8.0$  Hz, 1H), 8.31 (d,  $J = 7.6$  Hz, 2H), 7.82 (d,  $J = 7.6$  Hz, 2H), 7.56–7.38 (m, 12H), 7.28 (dd,  $J = 13.1, 5.7$  Hz, 2H), 6.96 (t,  $J = 7.3$  Hz, 2H), 6.60 (t,  $J = 7.4$  Hz, 2H), 6.50 (d,  $J = 8.4$  Hz, 2H), 6.43 (t,  $J = 9.2$  Hz, 2H), 2.95 (s, 3H), 2.87 (s, 6H).  $^{13}\text{C}$  NMR (101 MHz,  $\text{CDCl}_3$ )  $\delta$  (ppm): 174.08, 173.27, 156.58, 143.33, 142.27, 140.97, 139.20, 138.93, 136.30, 136.00, 134.25, 134.10, 131.89, 131.32, 131.05, 128.79, 128.37, 127.84, 127.57, 127.22, 126.15, 125.79, 124.78, 120.69, 119.87, 114.71, 56.78, 22.41, 22.33. Elem. Anal. calcd for  $\text{C}_{49}\text{H}_{36}\text{N}_4$  C 86.44, H 5.33, N 8.23; found C 86.41, H 5.31, N 8.17. HRMS (FAB+): calcd for  $\text{C}_{49}\text{H}_{36}\text{N}_4$   $[\text{M}]^+$ : 680.2940; found: 680.2940.

#### 4.6.8. Synthesis of 10-(4-(4,6-bis(4-methoxy-2-methylphenyl)-1,3,5-triazin-2-yl)-3-methylphenyl)-10H-spiro[acridine-9,9'-fluorene] (motmTrSAc)

A mixture of 2-chloro-4,6-bis(4-methoxy-2-methylphenyl)-1,3,5-

triazine (**8**) (514 mg, 1.44 mmol), (2-methyl-4-(10H-spiro[acridine-9,9'-fluorene]-10-yl)phenyl)boronic acid (**5**) (805 mg, 1.73 mmol), tetrakis(triphenylphosphine)palladium(0) (81 mg, 0.07 mmol) and potassium carbonate (400 mg, 2.88 mmol) in toluene (14 mL) and water (3 mL) was refluxed overnight under a nitrogen atmosphere. The reaction mixture was then filtered through a pad of silica and extracted with chloroform. The organic layer was washed with water and brine, and dried using anhydrous sodium sulfate. The filtrate was concentrated *in vacuo* to give a crude mixture, which was purified by column chromatography ( $\text{SiO}_2$ ,  $\text{CHCl}_3$ : hexane = 1 : 1) to afford compound **motmTrSAc** (1 g, 94%) as a yellow solid.

$^1\text{H}$  NMR (400 MHz,  $\text{CDCl}_3$ )  $\delta$  (ppm): 8.51 (d,  $J = 8.0$  Hz, 1H), 8.38 (d,  $J = 8.7$  Hz, 2H), 7.80 (d,  $J = 7.5$  Hz, 2H), 7.50 (d,  $J = 9.7$  Hz, 2H), 7.44 (d,  $J = 7.5$  Hz, 2H), 7.37 (t,  $J = 7.4$  Hz, 2H), 7.29–7.24 (m, 2H), 6.94 (td,  $J = 8.6, 1.7$  Hz, 4H), 6.88 (d,  $J = 2.4$  Hz, 2H), 6.57 (t,  $J = 7.5$  Hz, 2H), 6.48 (d,  $J = 8.3$  Hz, 2H), 6.41 (dd,  $J = 7.8, 1.2$  Hz, 2H), 3.89 (s, 6H), 2.91 (s, 3H), 2.88 (s, 6H).  $^{13}\text{C}$  NMR (101 MHz,  $\text{CDCl}_3$ )  $\delta$  (ppm): 173.11, 172.85, 161.73, 156.58, 142.99, 141.99, 141.60, 141.00, 139.18, 136.80, 134.08, 133.93, 133.42, 128.65, 128.57, 128.35, 127.79, 127.54, 127.20, 125.78, 124.74, 120.63, 119.85, 117.24, 114.74, 111.51, 56.78, 55.34, 23.21, 22.28. Elem. Anal. calcd for  $\text{C}_{51}\text{H}_{40}\text{N}_4\text{O}_2$  C 82.68, H 5.44, N 7.56; found C 82.91, H 5.44, N 7.50. HRMS (FAB+): calcd for  $\text{C}_{51}\text{H}_{40}\text{N}_4\text{O}_2$   $[\text{M}]^+$ : 740.3151; found: 740.3160.

#### 4.6.9. Synthesis of 2-chloro-4,6-bis(4-methoxyphenyl)-1,3,5-triazine (**6**)

To a solution of magnesium (779 mg, 32.04 mmol), iodine (68 mg, 0.27 mmol) in anhydrous THF (26 mL), 1-bromo-4-methoxybenzene (5 g, 26.7 mmol) was added dropwise under inert conditions. After stirring at  $70^{\circ}\text{C}$  for 3 h, the mixture was cooled to room temperature. The resulting Grignard solution was added dropwise to a solution of cyanuric chloride (1.48 g, 8.01 mmol) in anhydrous THF (40 mL). When the addition was completed, the mixture was stirred at  $50^{\circ}\text{C}$  overnight and then cooled to room temperature. The mixture was poured into a 1 N HCl aqueous solution, and the organic layer was extracted with dichloromethane and then dried using anhydrous sodium sulfate. The filtrate was concentrated *in vacuo* to give a crude mixture, which was purified by column chromatography ( $\text{SiO}_2$ ,  $\text{CH}_2\text{Cl}_2$ : hexane = 2 : 1) to afford compound **6** (1.5 g, 58%) as a white solid.

$^1\text{H}$  NMR (400 MHz,  $\text{CDCl}_3$ )  $\delta$  (ppm): 8.54 (d,  $J = 8.9$  Hz, 4H), 6.99 (d,  $J = 8.9$  Hz, 4H), 3.89 (s, 6H).  $^{13}\text{C}$  NMR (101 MHz,  $\text{CDCl}_3$ )  $\delta$  (ppm): 172.50, 171.59, 163.98, 131.35, 126.97, 114.06, 55.48. HRMS (EI+): calcd for  $\text{C}_{17}\text{H}_{14}\text{ClN}_3\text{O}_2$   $[\text{M}]^+$ : 327.0775; found: 327.0772.

#### 4.6.10. Synthesis of 2-chloro-4,6-di-*o*-tolyl-1,3,5-triazine (**7**)

To a solution of magnesium (1.7 g, 70.2 mmol) and iodine (150 mg, 0.6 mmol) in anhydrous THF (60 mL), 1-bromo-2-methylbenzene (10 g, 58.5 mmol) was added dropwise under inert conditions. After stirring at  $70^{\circ}\text{C}$  for 3 h, the mixture was cooled to room temperature. The Grignard solution was added dropwise to a solution of cyanuric chloride (3.24 g, 17.6 mmol) in anhydrous THF (90 mL). When the addition was completed, the mixture was stirred at  $50^{\circ}\text{C}$  overnight and then cooled to room temperature. The mixture was poured into a 1 N HCl aqueous solution, and the organic layer was extracted with dichloromethane and then dried using anhydrous sodium sulfate. The filtrate was concentrated *in vacuo* to give a crude mixture, which was purified by column chromatography ( $\text{SiO}_2$ ,  $\text{CH}_2\text{Cl}_2$ : hexane = 1 : 1) to afford compound **7** (2.74 g, 53%) as a white solid.

$^1\text{H}$  NMR (499 MHz,  $\text{CDCl}_3$ )  $\delta$  (ppm): 8.20 (d,  $J = 7.9$  Hz, 2H), 7.46 (t,  $J = 6.9$  Hz, 2H), 7.35 (dd,  $J = 13.9, 7.5$  Hz, 4H), 2.74 (s, 6H).  $^{13}\text{C}$  NMR (101 MHz,  $\text{CDCl}_3$ )  $\delta$  (ppm): 175.50, 170.95, 139.62, 134.16, 132.06, 131.86, 131.56, 126.18, 22.25. HRMS (EI+): calcd for  $\text{C}_{17}\text{H}_{14}\text{ClN}_3$   $[\text{M}]^+$ : 295.0876; found: 295.0876.

#### 4.6.11. Synthesis of 2-chloro-4,6-bis(4-methoxy-2-methylphenyl)-1,3,5-triazine (8)

To a solution of magnesium (729 mg, 30 mmol) and iodine (63 mg, 0.25 mmol) in anhydrous THF (24 mL), 1-bromo-4-methoxy-2-methylbenzene (5 g, 25 mmol) was added dropwise under inert conditions. After stirring at 70 °C for 3 h, the mixture was cooled to room temperature. The Grignard solution was added dropwise to a solution of cyanuric chloride (1.4 g, 7.5 mmol) in anhydrous THF (38 mL). When the addition was completed, the mixture was stirred at 50 °C overnight and then cooled to room temperature. The mixture was poured into a 1 N HCl aqueous solution, and the organic layer was extracted with dichloromethane and then dried using anhydrous sodium sulfate. The filtrate was concentrated *in vacuo* to give a crude mixture, which was purified by column chromatography (SiO<sub>2</sub>, CH<sub>2</sub>Cl<sub>2</sub>: hexane = 2 : 1) to afford compound **8** (1.47 g, 55%) as a white solid.

<sup>1</sup>H NMR (400 MHz, CDCl<sub>3</sub>) δ (ppm): 8.28 (d, *J* = 8.7 Hz, 2H), 6.90–6.76 (m, 4H), 3.86 (s, 6H), 2.75 (s, 6H). <sup>13</sup>C NMR (101 MHz, CDCl<sub>3</sub>) δ (ppm): 174.36, 170.40, 162.35, 142.44, 133.81, 126.72, 117.42, 111.52, 55.32, 23.19. HRMS (EI<sup>+</sup>): calcd for C<sub>19</sub>H<sub>18</sub>ClN<sub>3</sub>O<sub>2</sub> [M]<sup>+</sup>: 355.1088; found: 355.1089.

#### Conflicts of interest

There are no conflicts of interest to declare.

#### Acknowledgement

This work was supported by the NRF grant (No. 2018R1A2B2001293) funded by the MSIP. We thank the Samsung Display Co., Ltd for partial financial support.

#### Appendix A. Supplementary data

Supplementary data to this article can be found online at <https://doi.org/10.1016/j.dyepig.2019.107864>.

#### References

- Uoyama H, Goushi K, Shizu K, Nomura H, Adachi C. Highly efficient organic light-emitting diodes from delayed fluorescence. *Nature* 2012;492:234.
- Kwong RC, Sibley S, Dubovoy T, Baldo M, Forrest SR, Thompson ME. Efficient, saturated red organic light emitting devices based on phosphorescent platinum(II) porphyrins. *Chem Mater* 1999;11(12):3709–13.
- Chou P-T, Chi Y. Phosphorescent dyes for organic light-emitting diodes. *Chem Eur J* 2007;13(2):380–95.
- Zhu M, Yang C. Blue fluorescent emitters: design tactics and applications in organic light-emitting diodes. *Chem Soc Rev* 2013;42(12):4963–76.
- Yang Z, Mao Z, Xie Z, Zhang Y, Liu S, Zhao J, et al. Recent advances in organic thermally activated delayed fluorescence materials. *Chem Soc Rev* 2017;46(3):915–1016.
- Fu H, Cheng Y-M, Chou P-T, Chi Y. Feeling blue? Blue phosphors for OLEDs. *Mater Today* 2011;14(10):472–9.
- Zhang Q, Li J, Shizu K, Huang S, Hirata S, Miyazaki H, et al. Design of efficient thermally activated delayed fluorescence materials for pure blue organic light emitting diodes. *J Am Chem Soc* 2012;134(36):14706–9.
- Lee J, Shizu K, Tanaka H, Nomura H, Yasuda T, Adachi C. Oxadiazole- and triazole-based highly-efficient thermally activated delayed fluorescence emitters for organic light-emitting diodes. *J Mater Chem C* 2013;1(30):4599–604.
- Wu S, Aonuma M, Zhang Q, Huang S, Nakagawa T, Kuwabara K, et al. High-efficiency deep-blue organic light-emitting diodes based on a thermally activated delayed fluorescence emitter. *J Mater Chem C* 2014;2(3):421–4.
- Chen W-C, Lee C-S, Tong Q-X. Blue-emitting organic electrofluorescence materials: progress and prospective. *J Mater Chem C* 2015;3(42):10957–63.
- Saxena K, Jain VK, Mehta DS. A review on the light extraction techniques in organic electroluminescent devices. *Opt Mater* 2009;32(1):221–33.
- Brütting W, Frisichen J, Schmidt TD, Scholz BJ, Mayr C. Device efficiency of organic light-emitting diodes: progress by improved light outcoupling. *Phys Status Solidi A* 2013;210(1):44–65.
- Endo A, Sato K, Yoshimura K, Kai T, Kawada A, Miyazaki H, et al. Efficient up-conversion of triplet excitons into a singlet state and its application for organic light emitting diodes. *Appl Phys Lett* 2011;98(8):083302.
- Senes A, Meskers SCJ, Greiner H, Suzuki K, Kaji H, Adachi C, et al. Increasing the horizontal orientation of transition dipole moments in solution processed small molecular emitters. *J Mater Chem C* 2017;5(26):6555–62.
- Frischisen J, Yokoyama D, Endo A, Adachi C, Brütting W. Increased light out-coupling efficiency in dye-doped small molecule organic light-emitting diodes with horizontally oriented emitters. *Org Electron* 2011;12(5):809–17.
- Yokoyama D. Molecular orientation in small-molecule organic light-emitting diodes. *J Mater Chem* 2011;21(48):19187–202.
- Tanaka H, Shizu K, Miyazaki H, Adachi C. Efficient green thermally activated delayed fluorescence (TADF) from a phenoxazine–triphenyltriazine (PXZ–TRZ) derivative. *Chem Commun* 2012;48(93):11392–4.
- Hirata S, Sakai Y, Masui K, Tanaka H, Lee SY, Nomura H, et al. Highly efficient blue electroluminescence based on thermally activated delayed fluorescence. *Nat Mater* 2014;14:330.
- Wada Y, Shizu K, Kubo S, Suzuki K, Tanaka H, Adachi C, et al. Highly efficient electroluminescence from a solution-processable thermally activated delayed fluorescence emitter. *Appl Phys Lett* 2015;107(18):183303.
- Liu M, Komatsu R, Cai X, Hotta K, Sato S, Liu K, et al. Horizontally orientated sticklike emitters: enhancement of intrinsic out-coupling factor and electroluminescence performance. *Chem Mater* 2017;29(20):8630–6.
- Wada Y, Kubo S, Kaji H. Adamantyl substitution strategy for realizing solution-processable thermally stable deep-blue thermally activated delayed fluorescence materials. *Adv Mater* 2018;30(8):1705641.
- Chan C-Y, Cui L-S, Kim JU, Nakanotani H, Adachi C. Rational molecular design for deep-blue thermally activated delayed fluorescence emitters. *Adv Funct Mater* 2018;28(11):1706023.
- Jeong S, Lee Y, Kim JK, Jang D-J, Hong J-I. Non-doped thermally activated delayed fluorescent organic light-emitting diodes using an intra- and intermolecular exciplex system with a meta-linked acridine–triazine conjugate. *J Mater Chem C* 2018;6(34):9049–54.
- Woo S-J, Kim Y, Kwon S-K, Kim Y-H, Kim J-J. Phenazasiline/spiroacridine donor combined with methyl-substituted linkers for efficient deep blue thermally activated delayed fluorescence emitters. *ACS Appl Mater Interfaces* 2019;11(7):7199–207.
- Lin T-A, Chatterjee T, Tsai W-L, Lee W-K, Wu M-J, Jiao M, et al. Sky-blue organic light emitting diode with 37% external quantum efficiency using thermally activated delayed fluorescence from spiroacridine-triazine hybrid. *Adv Mater* 2016;28(32):6976–83.
- Woo S-J, Kim Y, Kim Y-H, Kwon S-K, Kim J-J. A spiro-silafuorene–phenazasiline donor-based efficient blue thermally activated delayed fluorescence emitter and its host-dependent device characteristics. *J Mater Chem C* 2019;7(14):4191–8.
- Li W, Li B, Cai X, Gan L, Xu Z, Li W, et al. Tri-spiral donor for high efficiency and versatile blue thermally activated delayed fluorescence materials. *Angew Chem Int Ed* 2019;58(33):11301–5.
- Joo CW, Huseynova G, Yifei J, Yoo J-M, Kim YH, Cho NS, et al. Highly efficient solution-processed blue organic light-emitting diodes based on thermally activated delayed fluorescence emitters with spiroacridine donor. *J Ind Eng Chem* 2019;78:265–70.
- Li B, Li Z, Hu T, Zhang Y, Wang Y, Yi Y, et al. Highly efficient blue organic light-emitting diodes from pyrimidine-based thermally activated delayed fluorescence emitters. *J Mater Chem C* 2018;6(9):2351–9.
- Han C, Zhao Y, Xu H, Chen J, Deng Z, Ma D, et al. A simple phosphine–oxide host with a multi-insulating structure: high triplet energy level for efficient blue electrophosphorescence. *Chem Eur J* 2011;17(21):5800–3.
- Im Y, Kim M, Cho YJ, Seo J-A, Yook KS, Lee JY. Molecular design strategy of organic thermally activated delayed fluorescence emitters. *Chem Mater* 2017;29(5):1946–63.
- Sosorev AY, Nuraliev MK, Feldman EV, Maslennikov DR, Borschhev OV, Skorotetckiy MS, et al. Impact of terminal substituents on the electronic, vibrational and optical properties of thiophene–phenylene co-oligomers. *Phys Chem Chem Phys* 2019;21(22):11578–88.
- Moon C-K, Kim K-H, Lee JW, Kim J-J. Influence of host molecules on emitting dipole orientation of phosphorescent iridium complexes. *Chem Mater* 2015;27(8):2767–9.